OE Optical Engineering

RESEARCH PAPER

# Generating Bessel beams with an elastomeric replica of a weevil carapace

**Paz Victoria T. Ramos,[a,b] Michie Vianca D. De Vera,[a] and Raphael A. Guerrero[a,*]**

[a]Ateneo De Manila University, School of Science and Engineering, Department of Physics, Quezon City, Philippines

[b]Isabela State University, College of Science, Department of Natural and Applied Sciences, Isabela, Philippines

**ABSTRACT.** We generate a zero-order Bessel beam with a laser beam focused onto an elastomeric replica of a weevil carapace scale. Carapace surface structures are imprinted on an elastomeric cast via soft lithography. The output Bessel beam exhibits the expected properties of non-diffraction over a propagation range of 30 cm. The width of the central spot at a propagation distance of 25 cm is 296.8 $\mu$m, corresponding to a replicated weevil scale with a diameter of 64.3 $\mu$m acting as an annular slit. Self-healing of the beam after encountering a wire obstruction is also observed.



**Keywords:** biomimetics; Bessel beam; annular slit; soft lithography; elastomer

Paper 20240188G received Feb. 23, 2024; revised Jun. 11, 2024; accepted Jul. 4, 2024; published Jul. 23, 2024.

## 1 Introduction

Biomimetics, also known as bio-inspired engineering or biomimicry, has garnered significant attention in the field of optics. By studying the unique optical properties of natural systems, researchers have unlocked new opportunities for designing and fabricating advanced optical materials and devices, offering enhanced functionalities, improved performance, and novel capabilities.

One remarkable example is the development of anti-reflective coatings inspired by the moth eye structure, enabling improved vision in low-light conditions and reducing glare on lenses and other optical surfaces.[1,2] The mechanical and optical properties of pristine spider silk have been harnessed to create optical fibers that surpass the performance of natural spider silk.[3,4] Drawing inspiration from the compound eyes of arthropods, lenses with a wider field of view have been developed for use in cameras.[5] Furthermore, the process of photosynthesis in plants has inspired the replication of leaf surface morphology, leading to novel methods for efficient light harvesting.[6] Taking cues from the transparent hair layer found on water plants, such as *Salvinia* and *Pistia*, superhydrophobic flexible thin films have been introduced as transparent coatings for optoelectronic devices.[7] Colombian butterflies, *M. cypris* and *G. oto*, showcase awe-inspiring structural coloration, where the observed colors vary with viewing angle. This remarkable phenomenon serves as a guiding inspiration for the creation of innovative devices utilizing iridescence as angular filters.[8]

Bessel beams belong to a fascinating class of laser beams that possess unique propagation properties. Unlike more conventional Gaussian beams, Bessel beams exhibit an invariant intensity profile over long distances, demonstrating minimal diffraction[9] and self-healing/reconstruction capabilities.[10,11] These useful characteristics make Bessel beams highly desirable for a wide range of applications. They are utilized for optical trapping and manipulation of

*Address all correspondence to Raphael A. Guerrero, rguerrero@ateneo.edu

supermagnetic beads,[12] capturing and manipulating aerosol particles,[13] as well as handling particles with both low and high refractive indices.[14] Moreover, Bessel beams serve as valuable tools for laser materials processing[15] and glass cutting/drilling.[16] In the field of phakometry, Bessel beams have shown superiority over conventional phakometers, offering improved lens parameter estimation, brighter Purkinje images, and enhanced interobserver repeatability.[17]

Recent research has investigated the application of elastomeric materials in optics to create innovative optical devices. Elastomers, known for their flexibility and deformability, offer distinct advantages in optics, such as tunability, ease of fabrication, and compatibility with complex geometries. Studies have specifically highlighted the use of elastomers in the development of flexible lenses,[18,19] tunable diffraction gratings,[20] deformable annular slits,[21] and scalable and stretchable optical fibers.[22] Previous work has explored the replication of biological structures and textures, such as the intricate microstructure of a butterfly wing, on elastomeric surfaces to mimic optical functionalities found in nature.[23]

Using insect surface structures as templates to produce Bessel beams is motivated by many cases of naturally occurring diffractive elements having the ability to manipulate light, observed with surface structures of butterfly wings,[24] flying termite wings,[25] snake skin,[26] *Hibiscus trionum* petals,[27] and banana stems.[28] In addition, a biomimetic approach addresses significant challenges in fabricating annular slits, a process that typically requires high precision and uniformity, from elastomers, such as polydimethylsiloxane (PDMS). A deformable annular slit for generating elliptical Bessel beams was successfully fabricated through photolithography of a photoresist layer deposited on a PDMS substrate.[21] Photolithography has the disadvantage of being a fairly intricate technique, involving photoresist deposition, exposure, and development. The method also requires proper handling of potentially hazardous chemicals.

In this study, we focus on the fabrication of an elastomeric replica of a weevil carapace, specifically for the generation of Bessel beams. The weevil carapace of our sample consists of eyespots of tessellated circular scales of yellow, blue, and green iridescent colors. Weevil scales are observed to have well-defined circular shapes with prominent edges. Our work presents a novel and cost-effective method for generating Bessel beams using the weevil surface replica. To the best of our knowledge, there has been no previous research investigating the biomimetic replication of weevil carapaces for the purpose of generating Bessel beams. This study aims to address that gap and explore the potential of utilizing natural structures for advanced optical applications.

Our paper is structured as follows: Sec. 2 describes the surface structure and iridescence of the weevil. In Sec. 3, we present the fabrication process for the elastomeric weevil. Experimental results for generating Bessel beams via the weevil replica are discussed in Sec. 4. Section 5 contains a summary of the paper with our final remarks.

## 2 Surface Microstructures of the Weevil

Figure 1 features photographs of the actual weevil used in this study, *Pachyrhynchus congestus ocellatus (P. c. ocellatus)*, a species indigenous to the Philippines. Taxonomically, *P. c. ocellatus* belongs to the order Coleoptera, encompassing beetles, and the superfamily Curculionoidea, consisting of weevils. This particular species is found in the northern region of Luzon, Philippines, and our specimen was obtained from a private seller for research purposes. *P. c. ocellatus* displays a glossy black appearance and exhibits relatively small, roundish eyespots, as reported by Schultze.[29] The eyespots have a concentric structure, consisting of an iridescent ring displaying a blue-green coloration, and are present on both the dorsal [Fig. 1(a)] and ventral [Fig. 1(b)] regions of the weevil's body.

Surface characteristics of the weevil are captured using a metallurgical system microscope (Olympus BX60M). Figure 2 presents micrographs of a dorsal eyespot at two levels of magnification. At 5× [Fig. 2(a)], the eyespots are seen to be composed of nearly circular tessellated scales. Visible iridescent colors include yellow, green, and blue. Increasing magnification to 10× in Fig. 2(b) reveals a clear delineation between the iridescent scales and the bulk black area of the carapace. We measure an average scale diameter of $64.8 \pm 3$ $\mu$m. Due to the curved shape of the specimen's surface, certain areas in the images are not in focus.

We note a smaller degree of curvature with the ventral section of the weevil carapace, leading to micrographs of an eyespot with higher magnifications in Fig. 3. Most of the image area

(a) (b)

**Fig. 1** Photographs of *Pachyrhynchus congestus ocellatus* (*P. c. ocellatus*), a weevil species native to the Philippines, in its natural form (habitus). Both the (a) dorsal and (b) ventral surfaces feature distinct annular blue-green eyespots that exhibit iridescence.

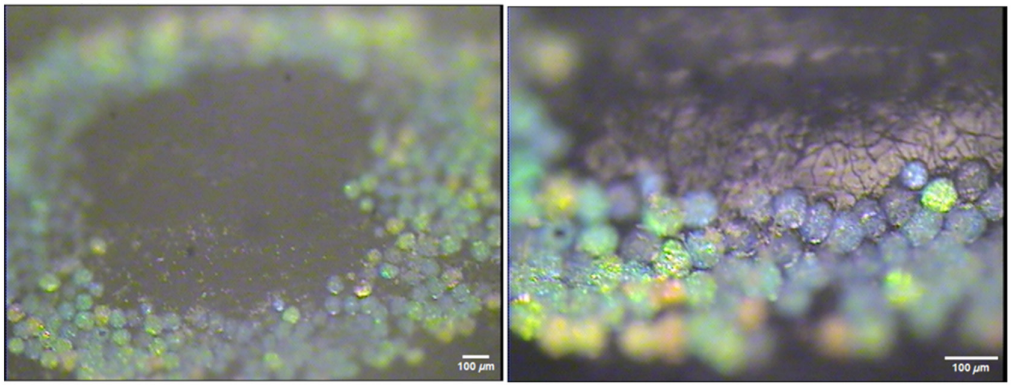


(a) (b)

**Fig. 2** Optical micrographs of an iridescent eyespot seen on the dorsal side of *P. c. ocellatus* at (a) 5× and (b) 10× magnifications.

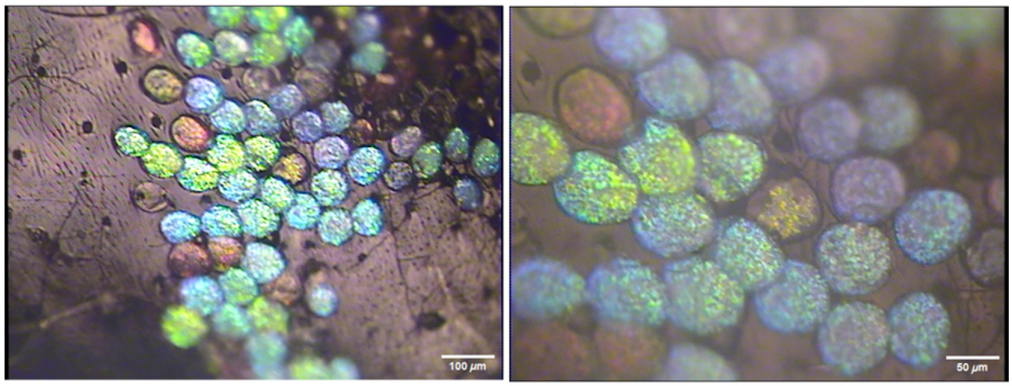


(a) (b)

**Fig. 3** Optical micrographs of an iridescent eyespot present on the ventral side of *P. c. ocellatus* at (a) 10× and (b) 20× magnifications.

appears in focus at 10× [Fig. 3(a)], indicating a relatively flat region. The color range of iridescence is similar to that of the ventral side. With 20× magnification in Fig. 3(b), scales are seen to have well-defined circular shapes with prominent edges. The average scale diameter for the ventral side is $65.1 \pm 0.9$ $\mu$m. The dimensions and form of the weevil scales are compatible with a biomimetic annular microstructure that may be fabricated through soft lithography.

## 3 Soft Lithographic Fabrication of a Biomimetic Elastomeric Replica

Soft lithography allows the replication of surface features by casting an elastomer onto a master template or mold. The process is known for its high fidelity, with the capability to copy structures at the nanoscale.[30] We have previously applied soft lithography in the preparation of elastomeric gratings based on PDMS[20,31,32] and chitosan.[33]

A mold is constructed from a plexiglass slab measuring 200 mm × 35 mm. Two recesses, each with dimensions 45 mm × 25 mm × 2 mm, are built into the slab for containing liquid PDMS. A weevil carapace is inserted, with the dorsal side exposed, at the bottom of one recess through a cutout. A second carapace for ventral features is installed in the other recess in a similar fashion. Both weevil samples are sealed into the mold with adhesive. The same adhesive seal is applied to the walls of the recesses to make them watertight. Figure 4(a) is a photograph of the final mold with the dorsal and ventral weevil surfaces oriented to come in contact with PDMS.

PDMS, prepared using a 10:1 mix of liquid prepolymer and curing agent, is poured over both weevil surfaces until the recesses are completely filled. The elastomer within the mold then undergoes degassing in a vacuum chamber for ∼6 h to remove any trapped air. Curing proceeds at an ambient temperature of 25°C for 6 days. Once fully cured, the PDMS layer is carefully peeled off from the mold, yielding elastomer casts with inverted surface profiles that are complementary to the original weevil surfaces. The products of the replication process are shown in Fig. 4(b) (dorsal surface) and Fig. 4(c) (ventral surface). For both surfaces, soft lithography is able to replicate the overall shape of the weevil carapace and its macroscopic structures. Iridescent coloration is absent in the elastomeric replicas due to the limited penetration of PDMS into the interior of the scales.[23] Details of replicated weevil structures are visible in the enlarged view of the ventral surface replica in Fig. 4(d). These include the coxa present in the thorax and abdomen, as well as the ventrites situated in the abdomen.

Figure 5 compares surface structures of the original weevil carapace with those of the PDMS replicas. The actual dorsal scales in Fig. 5(a) are effectively copied onto PDMS [Fig. 5(b)], with the elastomeric replicas maintaining the circular shapes seen on the original carapace. The average diameter for the replicated scales on this side of the carapace is $63.4 \pm 2.4$ $\mu$m, differing by only 1.7% from the original dimensions. Weevil scales found on the ventral carapace [Fig. 5(c)] are also successfully replicated by the soft lithography process, with corresponding surface

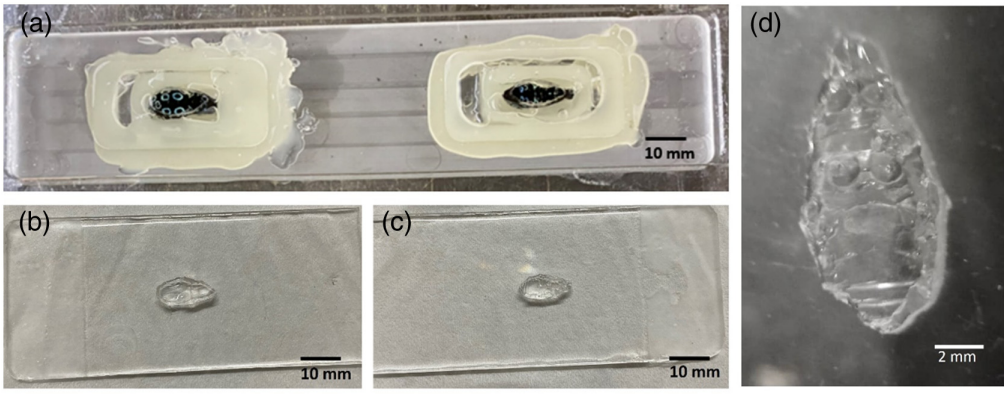


**Fig. 4** Soft lithographic replication of surface structures found on the weevil *P. c. ocellatus*: (a) a custom mold with master dorsal (left) and ventral (right) carapaces affixed; fabricated PDMS casts of the (b) dorsal and (c) ventral surfaces with inverted features and curvature after a single transfer step; (d) details of the ventral weevil carapace are clearly visible.

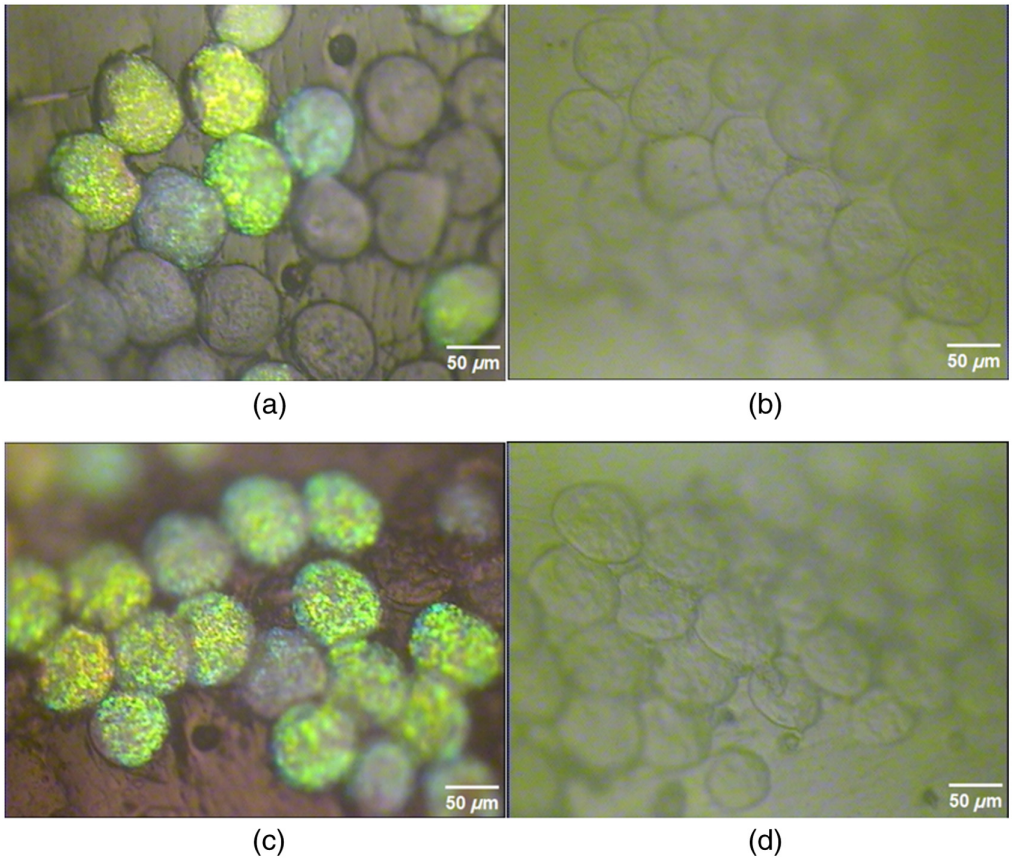


**Fig. 5** Optical micrographs at 20× magnification confirming the faithful replication of *P. c. ocellatus* carapace surface structures: (a) actual weevil scales and (b) PDMS replicas on the dorsal side; (c) actual weevil scales and (d) PDMS replicas on the ventral side.

features visible in Fig. 5(d). Deviating from the original measurements by only 1.3%, the PDMS scales are also circular with an average diameter of $64.3 \pm 3.5$ $\mu$m. Minor deviations in scale diameter between the weevil surface and its replica are attributed to slight deformation of the PDMS during curing. Our results in copying the carapace features of *P. c. ocellatus* are consistent with previous reports on employing PDMS-based soft lithography to replicate surface microstructures of the beetle *C. cobaltina*[34] and plant leaves.[35] The microscopic annular structures imprinted on the PDMS cast make possible the generation of Bessel beams through an optical system based on an annular slit and focusing lens.[36]

## 4 Bessel Beam Generation with a Replicated Weevil Scale

Bessel beams are commonly generated in experiments by directing light through an annular slit with diameter $d$ and a lens with focal length $f$. Our method for producing Bessel beams with a biomimetic PDMS replica of a weevil carapace employs the modified optical system illustrated in Fig. 6. Plane waves are incident on a single replicated scale with diameter $d$. The edge of the scale appears as a ridge protruding from the substrate due to the complementary nature of the elastomeric cast. This annular structure with microscopic dimensions serves as an obstacle to waves that are subsequently diffracted. We assume the thickness of the ridge to be much smaller than $d$. A focusing lens is placed a distance $f$ from the scale and the output is a collection of plane waves traveling on the surface of a cone. A Bessel beam is formed from the interference of these waves within a region of overlap after the lens. Light also simply passes through the transparent elastomer but transmitted waves do not contribute to the interference that produces a Bessel beam.

According to Durnin et al.,[9,36] the electric field of a zero-order Bessel beam, as modulated by the zero-order Bessel function $J_o$, is expressed as

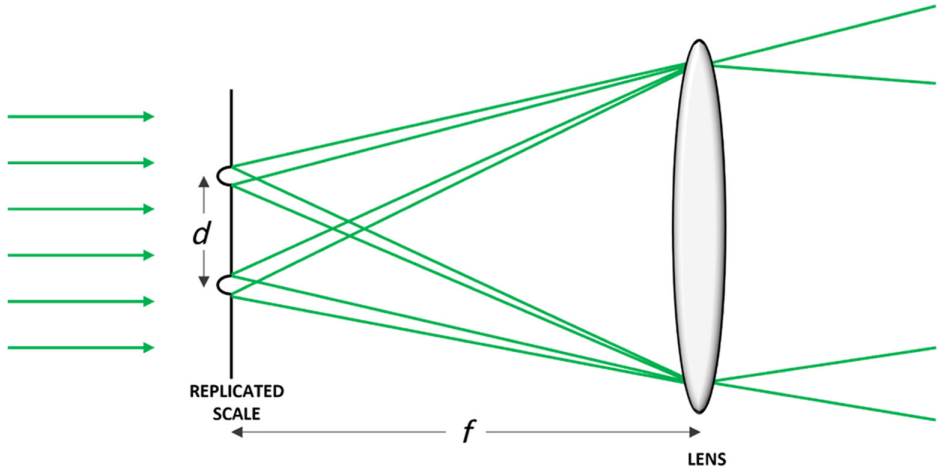


**Fig. 6** A Bessel beam is generated from plane waves diffracted by a circular elastomeric scale replica with diameter $d$. After the lens with focal length $f$, the waves interfere while traveling on the surface of a cone. Not shown are waves transmitted through the transparent surface of the elastomer.

$$E(r,z) = J_o(k_r r)e^{i\mathbf{k_z}\cdot\mathbf{z}}, \tag{1}$$

where $\mathbf{z}$ is the (longitudinal) propagation distance, $J_o(k_r r)$ is the zeroth-order Bessel function in terms of transverse coordinate $r = \sqrt{x^2+y^2}$, and $\mathbf{k_z}$ and $\mathbf{k_r}$ are the longitudinal and transverse wave vectors, respectively, with magnitudes $k_z = k\cos\alpha$ and $k_r = k\sin\alpha$, where $k = 2\pi/\lambda$. Equation (1) describes a Bessel beam as a continuous superposition of plane waves with wavelength $\lambda$ whose wave vectors lie on the surface of a cone with fixed opening angle $\alpha = \tan^{-1}(d/2f)$.[37] The intensity of a Bessel beam is proportional to

$$I(r,z) = J_0^2(k_r r), \tag{2}$$

and is independent of propagation distance.[38] Due to the conical distribution of wave vectors, a Bessel beam becomes capable of reconstructing its profile after encountering an obstruction. As described by Eq. (2), a zero-order Bessel beam appears as a central spot surrounded by concentric rings. Non-diffraction of the Bessel beam is typically manifested in experiments as the diameter of the central maximum remaining constant over a significant distance. The propagation-invariant core radius $\rho_0$ is given as

$$\rho_0 = \frac{2.405}{k\sin\alpha}, \tag{3}$$

with the value 2.405 related to the first minimum of $J_o$.[39] We perform experiments to confirm the above properties of Bessel beams created via the biomimetic replica.

## 5 Optical System Details and Experimental Results

Figure 7 is a schematic diagram of our optical setup for generating Bessel beams with the elastomeric carapace replica. An Ar+ laser (Modu-Laser) operating at a wavelength $\lambda = 514$ nm and

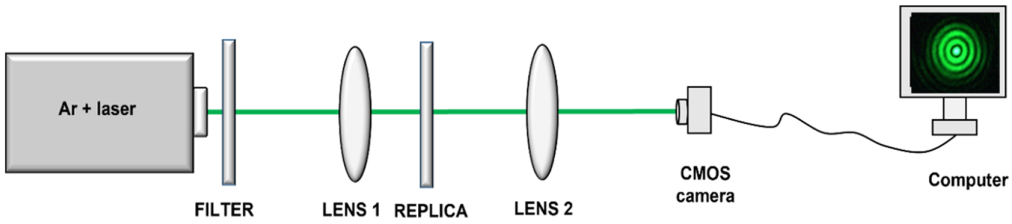


**Fig. 7** An optical system for generating Bessel beams based on an annular slit-lens configuration. Instead of an annular slit, we employ a replicated weevil scale as a circular microstructure.

output power of 25 mW serves as the light source. The beam passes through lens 1 with $f = 2.5$ cm and is incident on the replica, mounted on a custom holder located at the focal plane. We employ a replica of the ventral carapace due to its relatively flat surface that allows for more convenient alignment of the beam. The laser beam has a diameter of ~1 mm. As in Fig. 6, our aim with focusing the beam is to isolate one of the circular scales ($d \sim 60$ $\mu$m) imprinted on the elastomer. This involves carefully scanning the surface of the replica until an appropriate output intensity profile is observed on a screen placed after the elastomeric carapace. We assume paraxial behavior of the beam near the focal point of lens 1. Once an ideal scale structure has been found, lens 2 ($f = 5$ cm) is positioned a focal length from the replica. We capture images with a 4.92 MP CMOS camera (Industrial IDS), with a sensor size of 5.6 mm × 4.2 mm, positioned after lens 2. The camera is mounted on a track and connected to a computer system for monitoring generated Bessel beams. Our setup uses a neutral density filter to avoid image saturation. Bessel beam intensity profiles are recorded at various propagation distances $z$, with lens 2 at $z = 0$. To verify the self-healing capability of the experimental Bessel beams, a thin wire obstacle with a diameter of 223 $\mu$m is placed 5 cm after lens 2 and the resulting intensity profiles are recorded at different $z$ values.

With correct alignment of the incident laser beam, the circular structure of a replicated weevil scale produces a well-defined Bessel beam profile over a propagation range of 30 cm. Figure 8 presents a pair of Bessel beam intensity cross-sections captured at $z = 10$ cm and $z = 25$ cm. The experimental output beams exhibit the expected central spot and concentric maxima but only four rings are completely formed. Applying experimental parameters for $\alpha$ and $k$ in Eq. (3) yields a theoretical central spot width of 306 $\mu$m. At a propagation distance of 10 cm, we measure a core diameter of 323 ± 2.6 $\mu$m. The observed value is consistent with a Bessel beam produced by an annular slit with $d = 64.3$ $\mu$m, the mean diameter of a replicated ventral scale, and deviates from the expected value by only 5.6%. Variation in the distribution of rings is evident as the beam propagates farther and the outer maxima begin to degrade at $z = 25$ cm. At this distance the core diameter is 296.8 ± 2 $\mu$m, smaller by 8.4% after the beam travels 15 cm. We note that the core diameter begins decreasing rapidly after $z = 40$ cm, where the central spot width is now 252 ± 2.2 $\mu$m (a reduction of 22% from the diameter at $z = 10$ cm), with the Bessel beam reaching its maximum propagation distance.[36,37]

In Fig. 9, the experimental Bessel beam intensity profile is compared with a theoretical zero-order Bessel function calculated from the parameters of our optical system. We obtain the intensity values from the cross-section of a Bessel beam at $z = 10$ cm [Fig. 9(a)] and $z = 25$ cm [Fig. 9(b)]. At both distances, measured intensity is in good agreement with the calculated profile, with maxima and minima occurring at the expected locations along the beam radius. In Fig. 9(b), misalignment of intensity peaks and levels for the second ring is observed at a propagation distance of 25 cm as the beam begins to degrade. Experimental intensities of concentric rings are generally higher than computed levels. Deviations from theory are attributed to the weevil scale replica not having a perfectly circular shape. Transmission through the bulk

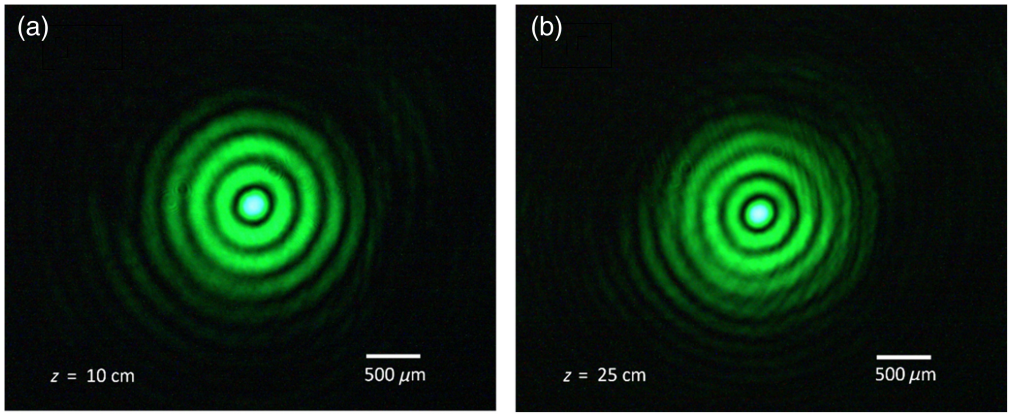


**Fig. 8** Bessel beams generated by an annular microstructure copied from a weevil carapace, with transverse intensity profiles recorded at (a) $z = 10$ cm and (b) $z = 25$ cm.

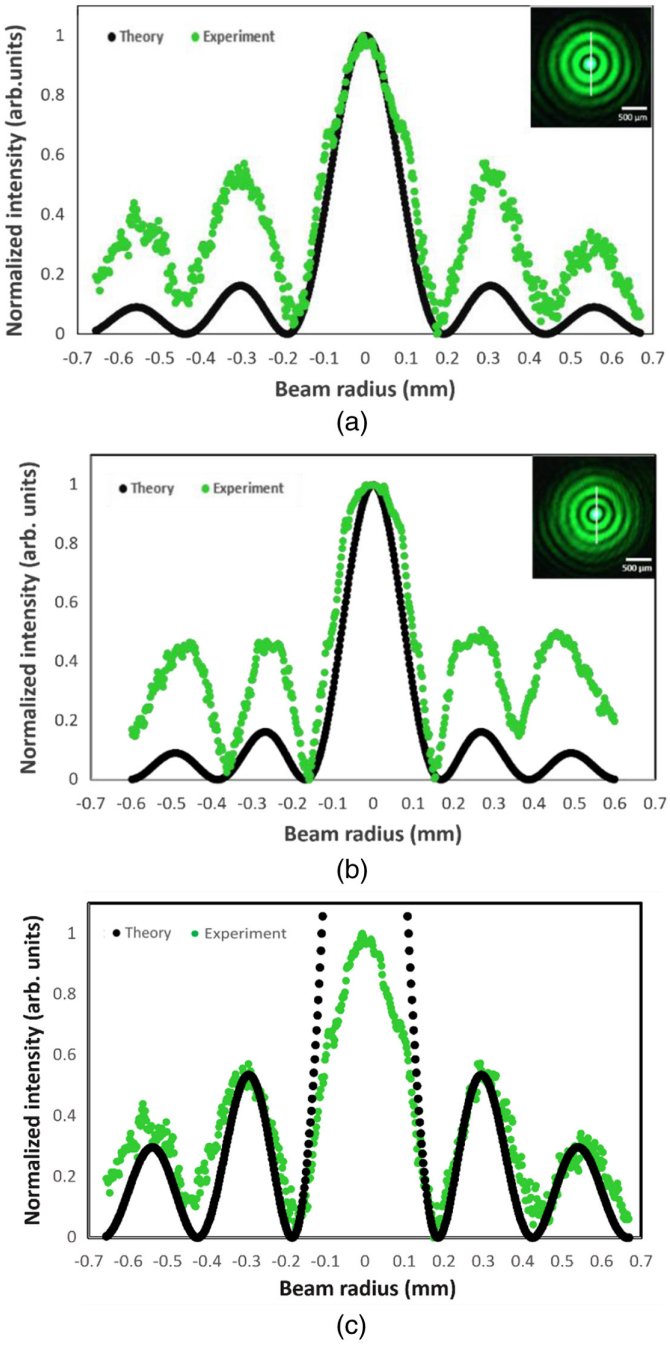


**Fig. 9** The intensity cross-sections (insets) of an output beam at (a) $z = 10$ cm and (b) $z = 25$ cm correspond to a zero-order Bessel function. An amplitude that is 1.8 times larger than the expected value yields (c) an improved overlap between theory and experimental data for the first two rings at $z = 10$ cm.

elastomer in the vicinity of the diffracting scale may also be a source of the higher background intensity. By increasing the amplitude of the $J_o$ function, the theoretical curve is a better match to the experimental behavior of the first and second rings of the Bessel beam. The data points in Fig. 9(c), for a Bessel beam at $z = 10$ cm, have side lobe intensities corresponding to a $J_o$ amplitude that is 1.8 times larger than the expected value applied in Fig. 9(a). We attribute the higher peaks of the concentric maxima to imperfections in the annular shape of the replicated scale leading to a nonuniform region of overlapping plane waves after the focusing lens in Fig. 6. Asymmetry in the conical distribution of wave vectors prevents interfering plane waves from generating outer rings. The 80% increase in amplitude of the Bessel beam side lobes is the result

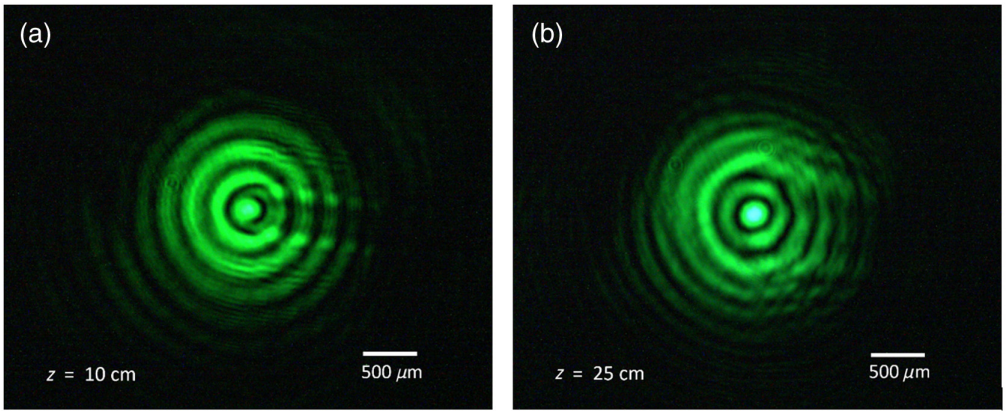


**Fig. 10** Self-healing in a Bessel beam produced with an elastomeric carapace replica: (a) the intensity is distorted by an obstacle at a propagation distance of 10 cm but (b) recovery of the core and first ring is achieved with the beam at 25 cm.

of energy being localized in the interior rings. For the propagation distance reported here, the experimental behavior of the Bessel beam core is unaffected by the reduced number of concentric rings, with the amplitude of the central maximum noticeably smaller than the predicted level in Fig. 9(c).

Bessel beams produced by the elastomeric carapace replica demonstrate a self-healing ability (Fig. 10). In Fig. 10(a), a prominent shadow of the wire obstacle placed 5 cm after lens 2 is visible in the beam profile recorded at $z = 10$ cm. The central spot is distorted and gaps are present in the concentric rings. Due to the conical distribution of wave vectors, light that bypasses the obstacle is able to reconstruct the central spot and rings as the beam continues to propagate. The core and first ring are fully restored at $z = 25$ cm in Fig. 10(b). Degradation of the outer rings is due to the fixed amount of energy available for self-healing from regions of the beam that did not encounter the wire obstruction.

## 6 Conclusion

We report the successful generation of zero-order Bessel beams with an elastomeric replica of a weevil (*P. c. ocellatus*) carapace. The carapace replica is fabricated through soft lithography with PDMS and is imprinted with biomimetic circular microstructures copied from weevil scales. Bessel beams are produced in experiments where an elastomeric scale replica performs the same action as an annular slit. Output Bessel beams exhibit non-diffraction, with the core diameter decreasing by only 23% over a range of 30 cm. Width of the central spot is consistent with a circular aperture having $d = 64.3$ $\mu$m, the average diameter of a replicated scale. Intensity cross-sections of an experimental beam correspond to the expected zero-order Bessel function. Our beams are also capable of self-healing after a wire obstacle.

Our results provide further evidence of optical applications made possible by biomimetic structures. Bessel beams may be produced with apertures replicated from surface features found in nature through soft lithography, without the need for more complex and expensive techniques involving micromachining or chemical etching. Bessel beams from the elastomeric carapace should be appropriate for materials processing or micromanipulation, once specific propagation properties are established.

### Disclosures

The authors have no relevant financial interests in the paper and no other potential conflicts of interest to disclose.

### Code and Data Availability

Data utilized in this study are available from the authors upon request.

## Acknowledgments

P.V. Ramos acknowledges support from the Commission on Higher Education (Philippines) K to 12 Transition Program and the Graduate Assistant scholarship of Ateneo de Manila University. R.A. Guerrero is the current holder of the College 1980 Fr Jose Ramon T Villarin, SJ Professorial Chair. Equipment grants were provided by the Philippine Council for Industry, Energy, and Emerging Technology Research and Development (PCIEERD) and the IR 4.0 Research Program of the Ateneo Research Institute of Science and Engineering (ARISE).

## References

1. S. Park et al., "Fabrication and characterization of moth-eye mimicking nanostructured convex lens," *Microelectron. Eng.* **158**, 35–40 (2016).
2. T. Yano, H. Sugawara, and J. Taniguchi, "Moth-eye structured mold using sputtered glassy carbon layer for large-scale applications," *Micro Nano Eng.* **9**, 100077 (2020).
3. K. Hey Tow et al., "Exploring the use of native spider silk as an optical fiber for chemical sensing," *J. Lightwave Technol.* **36**(4), 1138–1144 (2018).
4. J. Li et al., "Spider silk-inspired artificial fibers," *Adv. Sci.* **9**(5), 2103965 (2022).
5. Y. Song et al., "Digital cameras with designs inspired by the arthropod eye," *Nature* **497**, 95–99 (2013).
6. Z. Huang et al., "Replication of leaf surface structures for light harvesting," *Sci. Rep.* **5**, 14281 (2015).
7. F. Vüllers et al., "Bioinspired superhydrophobic highly transmissive films for optical applications," *Small* **12**(44), 6144–6152 (2016).
8. C. P. Barrera-Patiño et al., "Photonic effects in natural nanostructures on *Morpho cypris* and Greta oto butterfly wings," *Sci. Rep.* **10**, 5786 (2020).
9. J. Durnin, "Exact solutions for nondiffracting beams. I. The scalar theory," *J. Opt. Soc. Am. A* **4**, 651–654 (1987).
10. V. Garcés-Chávez et al., "Simultaneous micromanipulation in multiple planes using a self-reconstructing light beam," *Nature* **419**, 145–147 (2002).
11. Z. Bouchal, J. Wagner, and M. Chlup, "Self–reconstruction of a distorted nondiffracting beam," *Opt. Commun.* **151**, 207–211 (1998).
12. U. M. S. Andrade, A. M. Garcia, and M. S. Rocha, "Bessel beam optical tweezers for manipulating superparamagnetic beads," *Appl. Opt.* **60**, 3422–3429 (2021).
13. A. E. Carruthers et al., "Selection and characterization of aerosol particle size using a Bessel beam optical trap for single particle analysis," *Phys. Chem. Chem. Phys.* **14**(19), 6741 (2012).
14. Z. Liu et al., "Simultaneous trapping of low-index and high-index microparticles using a single optical fiber Bessel beam," *Opt. Lasers Eng.* **131**, 106119 (2020).
15. R. Stoian et al., "Ultrafast Bessel beams: advanced tools for laser materials processing," *Adv. Opt. Technol.* **7**(3), 165–174 (2018).
16. C. Lutz et al., "Multi-Bessel beams generated by an axicon and a spatial light modulator for drilling applications," *Photonics* **10**(4), 413 (2023).
17. M. Suheimat et al., "Improvements to phakometry using Bessel beams," *Optom. Vis. Sci.* **94**(11), 1015–1021 (2017).
18. P. Liebetraut et al., "Elastomeric lenses with tunable astigmatism," *Light Sci. Appl.* **2**, e98 (2013).
19. S. Shian, R. M. Diebold, and D. R. Clarke, "Tunable lenses using transparent dielectric elastomer actuators," *Opt. Express* **21**, 8669–8676 (2013).
20. C. T. Pada and R. A. Guerrero, "Fluid-enhanced tunable diffraction with an elastomeric grating," *Opt. Eng.* **56**(5), 054101 (2017).
21. D. P. Guaña and R. A. Guerrero, "A deformable annular slit for generating elliptical Bessel beams," *Jpn. J. Appl. Phys.* **58**, 062002 (2019).
22. A. Leber et al., "Stretchable thermoplastic elastomer optical fibers for sensing of extreme deformations," *Adv. Funct. Mater.* **29**(5), 1802629 (2019).
23. S. H. Kang, T. Y. Tai, and T. H. Fang, "Replication of butterfly wing microstructures using molding lithography," *Curr. Appl. Phys.* **10**(2), 625–630 (2010).
24. K. Shuichi, Y. Shinya, and K. Kenji, "Mechanisms of structural colour in the Morpho butterfly: cooperation of regularity and irregularity in an iridescent scale," *Proc. R. Soc. Lond. B* **269**, 1417–1421 (2002).
25. M. P. Aji et al., "A unique diffraction pattern formed by a grating from a flying termite wing," *Phys. Educ.* **57**(5), 055026 (2022).
26. D. S. Dhillon et al., "Interactive diffraction from biological nanostructures," *Comput. Graph. Forum.* **33**(8), 177–188 (2014).
27. E. Moyroud et al., "Cuticle chemistry drives the development of diffraction gratings on the surface of *Hibiscus trionum* petals," *Curr. Biol.* **32**(24), 5323–5334.e6 (2022).

28. M. P. Aji et al., "A simple diffraction experiment using banana stem as a natural grating," *Phys. Educ.* **52**(2), 025009 (2017).
29. W. Schultze, "A monograph of the pachyrrhynchid group of the Brachyderinae, Curculionidae: Part I. The genus Pachyrrhynchus Germar," *Philipp. J. Sci.* **23**, 609–673 (1923).
30. M. Sun et al., "Artificial lotus leaf by nanocasting," *Langmuir* **21**, 8978–8981 (2005).
31. R. A. Guerrero et al., "Effects of spontaneous surface buckling on the diffraction performance of an Au-coated elastomeric grating," *Opt. Commun.* **270**(1), 1–7 (2007).
32. R. A. Guerrero and S. J. C. Oliva, "Optical wavelength tuning via actuation of a fluidic grating," *Opt. Eng.* **53**(2), 025104 (2014).
33. E. G. Gumayan, I. K. D. Dimzon, and R. A. Guerrero, "Chitosan from crab shell waste for soft lithography of bioplastic diffraction gratings," *Appl. Opt.* **62**(10), 2487–2492 (2023).
34. R. A. Guerrero and E. B. Aranas, "Diffraction from relief gratings on a biomimetic elastomer cast," *Mater. Sci. Eng. C* **30**(8), 1170–1174 (2010).
35. W. Wu et al., "Plant leaves as templates for soft lithography," *RSC Adv.* **6**, 22469–22475 (2016).
36. J. Durnin, J. Miceli, Jr., and H. Eberly, "Diffraction-free beams," *Phys. Rev. Lett.* **58**(15), 1499–1501 (1987).
37. M. Anguiano-Morales et al., "Conical dynamics of Bessel beams," *Opt. Eng.* **46** (7), 078001 (2007).
38. M. Duocastella and C. B. Arnold, "Bessel and annular beams for materials processing," *Laser Photonics Rev.* **6**(5), 607–621 (2012).
39. G. Milne, G. D. M. Jeffries, and D. T. Chiu, "Tunable generation of Bessel beams with a fluidic axicon," *Appl. Phys. Lett.* **92**(26), 261101 (2008).

**Paz Victoria T. Ramos** completed her undergraduate studies in physics-mathematics at the University of the Philippines Baguio. She then pursued a master's degree in physics at Ateneo de Manila University, where she is currently enrolled as a PhD student.

**Michie Vianca D. De Vera** received her bachelor's degree in applied physics with materials science and engineering from Ateneo de Manila University in 2020. She was awarded a post-graduate diploma in earth system physics from Abdus Salam International Centre for Theoretical Physics in 2021. She received her master's degree in atmospheric sciences from the University of Illinois at Urbana-Champaign, where she is presently pursuing her PhD.

**Raphael A. Guerrero** received his PhD in physics from the University of the Philippines Diliman, in 2005. Currently, he is the dean of the School of Science and Engineering at Ateneo de Manila University. He served as the president of the Physics Society of the Philippines in 2011 and 2012 and is a member of SPIE and Optica. In 2013, he was a recipient of the World Academy of Sciences Prize for Young Scientists in Developing Countries.